Journal of Magnetism and Magnetic Materials 522 (2021) 167542

Contents lists available at ScienceDirect

Journal of Magnetism and Magnetic Materials

journal homepage: www.elsevier.com/locate/jmmm

Strain-induced control of magnetocrystalline anisotropy energy in FeCo thin films

Michael Wolloch [a,b,*], Dieter Suess [b,c,d]

[a] Faculty of Physics, University of Vienna, Kolingasse 14-16, 1090 Vienna, Austria
[b] Christian Doppler Laboratory, Advanced Magnetic Sensing and Materials, University of Vienna, Währinger Strasse 17, 1090 Vienna, Austria
[c] Faculty of Physics, University of Vienna, Währinger Strasse 17, 1090 Vienna, Austria
[d] University of Vienna Research Platform MMM Mathematics – Magnetism – Materials, Faculty of Physics, University of Vienna, Austria

ARTICLE INFO

Keywords:
Magnetostriction
Magnetic anisotropy
FeCo alloys
DFT
Thin films

ABSTRACT

We use density functional theory calculations to compute the lateral strain dependence of the magnetocrystalline anisotropy (MCA) energy of thin FeCo films. We investigate the effect of lateral strain on the MCA energy especially in the context of magnetostriction, which needs to be minimized for some applications like GMR sensors. The magneto-elastic coupling responsible for magnetostriction is a strain-derivative of the MCA energy, thus we concentrate to find extrema in the MCA energy vs. strain curves, which we find for both ordered $Fe_{50}Co_{50}$ films, as well as for disordered $Fe_{10}Co_{90}$ films modeled by special quasirandom structures. We show that using lateral strain we can switch the easy axis of magnetization from out-of-plane to in-plane in many cases. We can furthermore use lateral strain in combination with the film-thickness to minimize magnetostriction and change the MCA energy at the same time.

1. Introduction

Magnetic thin films are used in many applications, from data storage to magnetic field sensors and magneto-caloric cooling [1,2]. The magnetic properties of a material are coupled to the elastic properties, which is especially important for extremely thin films (<5 nm), since they are more easily stretched or compressed. It has long been known that sufficiently thin films can even change their crystal structure conforming to that of the substrate due to the large interface-to-volume ratio, which is called pseudomorphism of thin films (see e.g. [3,4]). The magneto-elastic coupling leads to magnetostriction and the inverse effect, the Villari effect. This is e.g. a problem for giant magnetostriction (GMR) and tunnel magnetoresistance (TMR) sensors, in particular angle sensors. These show a large increase in angle errors if strain is put on the stack due to bending of the substrate or thermal effects [5]. FeCo alloys have long been of interest due to their high magnetic saturation values (see e.g. [6]), and thin FeCo films are typically used as ferromagnetic layers of such GMR and TMR angle sensors. However, significant modification in the magnetic parameters on such films are observed under strain [7].

Since magnetoelastic coupling energy is the strain derivative of the magnetic anisotropy energy, it may be large even if the magnetic anisotropy itself is small or zero. In fact, for GMR, one usually prefers a material with small magnetic anisotropy and large saturation magnetization. Small MCA energy is desirable, since it should be possible to drive the system into saturation with small applied fields, and a large magnetization is needed to transfer significant energy from the magnetic to the elastic system [8].

In this work we aim to analyze the possibilities of reducing the MCA energy of thin FeCo layers using pre-strains that might be applied using a different choice of substrate or interlayers in the GMR angle sensor stack. Since the used FeCo layers are extremely thin (~1 nm), a lateral stretching of the lattice by up to several percent is conceivable.

2. Computational methods

All computations are done with the density functional theory suite *Vienna Ab-Initio Simulation Package* VASP [9–11] version 5.4.1, using the Projector Augmented-Wave (PAW) method [12,13]. The plane wave energy cutoff was converged using 5 rescaled bulk cells of ordered bcc FeCo, ranging from 90% to 110%, of the trial volume 23 $Å^3$. The total energies of these 5 structures where fitted to a Birch-Murnaghan equation of state to obtain the lattice parameter and the bulk modulus for a starting cutoff energy of 200 eV [14]. This energy was increased in steps

* Corresponding author.
E-mail address: michael.wolloch@univie.ac.at (M. Wolloch).

https://doi.org/10.1016/j.jmmm.2020.167542
Received 14 August 2020; Received in revised form 15 October 2020; Accepted 30 October 2020
Available online 19 November 2020

of 10 eV, while repeating the total energy calculations and fitting procedure until the lattice parameter was converged to 0.5% and the bulk modulus to 1%. This procedure lead to a cutoff of 320 eV, about 9% larger than the suggested value for the used Fe_pv PAW potential and 19% greater than that of Co. These two potentials have a reference electron configuration of $3p^6, 3d^7$, and $4s^1$ ($3d^8, 4s^1$) for Fe (Co). Tests with potentials treating also 3*s* states (for Fe) and 3*s* and 3*p* states (for Co) as valence did not lead to a significant change in MCA energies. To avoid the effect of Pulay stresses during volume changing relaxations, the energy cutoff was increased to 500 eV for all relaxations.

The Brillouine zone was sampled with generalized Monkhorst-Pack grids as described by Wisesa and coworkers [15]. The distance between lattice points on the real-space superlattice, described by the parameter r_{min}, was set to 69.5 Å corresponding to a FeCo bulk cell total energy convergence of 0.1 meV. Since for some strains of the FeCo bulk, the MCA energy was different by a couple of percent if r_{min} was set to 75 Å for testing, but did not change if increased further, $r_{\text{min}} = 75$ Å was adopted for all MCA calculations (leading to ~14000 k-points in the unit cell of FeCo bulk), while relaxations where done at $r_{\text{min}} = 69.5$ Å.

To approximate the effects of exchange and correlation the generalized gradient correction (GGA) as parametrized by Perdew, Burke, and Ernzerhof (PBE) has been used [16]. It has been recently shown that GGAs are more accurate in the descriptions of the magnetism of transition metals than meta-GGAs functionals or the otherwise very successful SCAN functional [17].

To ensure accurate forces during relaxations we use an additional superfine fast Fourier transform (FFT) grid for the evaluation of the augmentation charges and a smearing of ≤ 0.1 eV according to Methfessel and Paxton [18] (first order). For total energy calculations the tetrahedron method with Blöchl corrections has been used [12]. In all total energy GGA calculations we explicitly account for non spherical contributions of the gradient corrections inside the PAW spheres. Electronic relaxations are converged to less than 10^{-4} meV, while forces in ionic relaxations where converged to ≤ 0.01 eV/Å.

While we disregard spin-orbit coupling for relaxations, it is naturally turned on for all calculations of the MCA. We also turn off symmetry options explicitly and compute the MCA by subtracted the total energy values of hard and easy axis orientation of the magnetic moments. MCA energies are defined as the difference between the out-of-plane direction to the in-plane direction, $E_{\text{MCA}} = E_{\perp} - E_{\parallel}$. Thus, negative values of E_{MCA} indicate that the c-direction (normal to the film surface) is the easy axis for the magnetization, while a positive value indicates that the in-plane orientation is more favorable. (Unless otherwise mentioned we disregard the possible differences for the in-plane energies (e.g. between the [110] and the [100]) since they are typically significantly smaller than the difference to the out-of-plane direction as soon as any lateral strain is involved. Without strain however, the in-plane anisotropy is experimentally found to dominate, at least for films of 40-120 nm thickness [19]).

To gain more information on the MCA we do not only calculate the total energy for magnetic moments pointing in- or out-of-plane, but also for 4 values in between. This allows us to fit the data to $E_{\text{MCA}} = K_1 \sin^2(\theta) + K_1 \sin^4(\theta)$, not only computing the anisotropy constant K_1 (for uniaxial anisotropy also often called K_u), but the higher order term K_2 as well.

3. Results and discussion

3.1. Bulk FeCo

We started our investigation by establishing a baseline for bulk FeCo in the *B*2 (CsCl prototype) structure. Using the Birch-Murnaghan equation of state (see Section 2) we determined the equilibrium lattice constant to be $a = 2.8475$ Å, less than half a percent smaller than the experimental value for equiatomic, ordered FeCo alloys of 2.8506 Å too 2.8570 Å [20]. This small discrepancy is explained by the fact that the calculation is performed at 0 K and the measurements are done at room temperature.

To investigate the dependence of the perpendicular magnetic anisotropy, we strain the bulk material evenly in the *x* and *y* direction, and find the corresponding z-parameter, by starting from the volume conserving value of *z*, and computing the total energy of *z* values a couple of percent higher and lower than that. The final *z* parameter of the cell is found by fitting a quadratic function to the total energy data and computing its minimum value. The MCA energy is then computed for each strain by turning the spins 90° from [001] to [110]. We chose this rotation (instead of [001]→[100]) so we are turning the magnetic moments through the [111] direction and can investigate the magnetic anisotropy for the unstrained cubic case thoroughly. At $c/a = 1$, the MCA energies are extremely small, with the [110] direction favored by ~0.8 μeV/formula unit (f.u.) with respect to the [001] direction (or equivalently [100] and [010]), and ~0.6 μeV/f.u. compared to the [111] direction. It has to be said that these energies are at the limit of the accuracy of our method and we cannot be sure that the results for the unstrained bulk are correct. Indeed, literature gives (at room temperature) the [111] direction as the easy axis, and the [110] as intermediate, opposite to our results [21], while the [001] direction is the hard axis also in literature.

Even for relatively small strains we observe that the MCA energy is many orders of magnitude larger than for the unstrained case. E_{MCA} also scales completely linear with lattice strain as can be seen in Fig. 1. (Since in our data K_2 is always smaller than K_1 by a factor of 100 to 1000, we report only K_1 here.) The easy axis for the magnetisation is the [001] direction for compressive strain, and the [110] axis if the material is stretched beyond its equilibrium lattice parameter in the *x* and *y* directions. The change in the easy axis is marked in Fig. 1 by the change of the background color from white to grey, and is easily understood from a geometrical point of view. If compressive strain is applied, the lattice vector normal to the strain-plane expands and thus we effectively introduce a tetragonal distortion with an elongated *z* axis. As has been shown previously, a tetragonal distortion can lead to very high MCA in FeCo alloys [22]. Experimentally such a distortion (on a smaller scale) is achieved by the addition of small ions like carbon or boron into the alloy, which occupies interstitial sites and the MCA is believed to be affected mainly by the introduced tetragonality and not hybridization with the dopant atoms [23–25].

If the lattice is expansively strained in the *x* and *y* direction, the

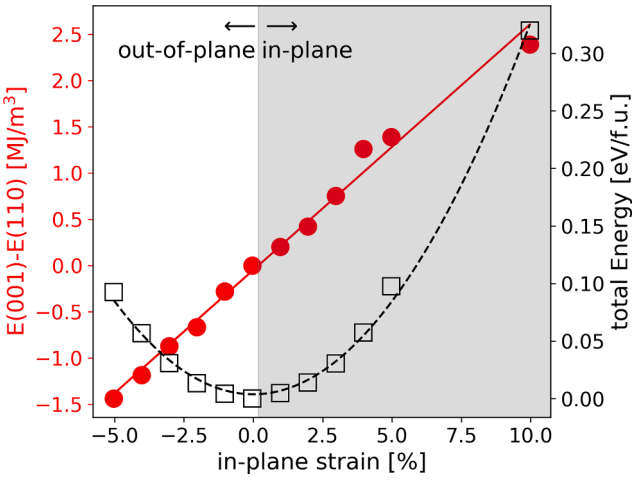

Fig. 1. MCA energy (filled circles, left y-axis) and total energy (empty squares, right y-axis) as a function of lateral strain in *a* and *b* direction of a fully ordered bcc FeCo bulk. The lines are linear and quadratic fits to the DFT data. The white and grey background indicate regions with the magnetic easy axis laying in the in-plane or out-of-plane direction.

tetragonal distortion is obviously of opposite sign, with a compressed z axis. This leads to a strongly favored [110] axis for the orientation of the magnetic moments, and the scaling appears to stay linear until a large in-plane strain of 10%. The magnetic moments themselves do not scale completely linear with strain, but show a maximum at $+1\%$ for Co and $+2\%$ for Fe. Overall the variation around the mean values of 1.74 μ_b and 2.79 μ_b for Co and Fe, respectively, is rather small however, from -2% to $+1\%$ for Co and -3% to $+2\%$ for Fe.

Since we observe a linear scaling (with a slope ~0.27 MJm^{-3} per percent of planar strain) for the bulk MCA of ordered bcc FeCo from -5% to $+10\%$, the magnetostriction should be constant over this large strain region.[1] At 10% strain the MCA has grown to ~2.4 MJ/m^3, which corresponds to 387 μeV/f.u. and is thus four orders of magnitude larger than the value of the unstrained bulk at ~0.6 μeV/f.u.. However, this is still less than halve compared to the ~1.5 meV/f.u. predicted by Burkert et al. for slightly more Co rich FeCo alloys at $c/a \simeq 1.22$ [22].

3.2. Thin stoichiometric FeCo slabs

Thin films are more interesting than the bulk case, but also more complex due to reduced symmetry and the interface with the substrate. Here we deal with unsupported, free-floating thin films, which are usually called slabs in computational modeling, of less than 2 nm thickness. Thus we do not deal explicitly with the interface to the substrate, although we consider the lateral strain it might introduce implicitly and the surfaces in the slab still break many symmetries of the bulk crystal, which changes the magnetic properties nevertheless. Depending on the chosen surface there might be different terminations possible, which may also influence the local magnetization and in turn the MCA. Furthermore, for those unsupported slabs, the equilibrium lattice parameter along the surface plane will change as well, depending on the slab thickness. This is an effect of surface energy, which is minimized by reducing the surface area and thus the in-plane lattice parameter. If the slab is relatively thick, this is compensated by the bulk-like inner region, but for slabs of less than 2 nm thickness the in-plane lattice parameter might shorten considerably.

In the following we will investigate fully ordered, stoichiometric $Fe_{50}Co_{50}$ slabs of various thicknesses with both 001, and 110 surfaces (see Fig. 2) For bcc structures, the 110 surface is commonly found to be the lowest energy surface [26], and indeed we find a lower surface energy $\sigma_{110} = 0.12\,J/m^2$ for the 110 surface than for the 100 surface at $\sigma_{110} = 0.20\,J/m^2$. The surface energy was computed for slabs of ~1.5 nm thickness as

$$\sigma = \frac{1}{2A}\left(\frac{E_{slab}}{N_{slab}} - \frac{E_{bulk}}{N_{bulk}}\right), \tag{1}$$

where A is the cross section area of the cell, E is the total energy, and N is the number of atoms in a given structure. (For the 100 surface of a stoichiometric FeCo slab, both Fe and Co terminated surfaces are present (see Fig. 2(b)), so the surface energy in that case is the average of both, while the 110 surface contains both species and is equivalent on both sides of the slab (see Fig. 2(c)))

In practice however, the seeding layer and method of deposition allows bcc FeCo to grow both in the 110 (see e.g. [7,27] or the 001 direction (e.g. [25,28]).

The atomic positions of all atoms are allowed to relax for each applied lateral strain before the MCA is computed.

3.2.1. Ordered stoichiometric 001 slabs

As before we compute the MCA energy (the K_1 constant) of the system by rotating the magnetization axis from the [001] to the [110] direction, from the surface normal into the surface plane. In Fig. 3 we can see that at strains between 7% and 10% (lateral lattice parameter between 3.0 and 3.1 Å) the MCA energy has a maximum for both the 7.5 Å and 15 Å thick films, although the exact location depends on the smoothing parameters of the splines used to fit the data. Nevertheless, the clear existence of local extrema for both slabs indicate the possibility to minimize magnetostriction in FeCo 001 slabs with reasonable pre-straining. At these strains we find a large MCA with in-plane easy axis.

We can furthermore see that the transition of the easy axis from the out-of-plane to the in-plane direction is no longer at 0% strain, but at about 4.2% for the thinner and 2.2% for the thicker film. This clearly shows that the surfaces themselves has a sizable contribution to the MCA. However, the inversion happens at lateral lattice parameters that differ by less than 1% (2.876 Å for the thinner film and 2.856 Å for the thicker one). For a thinner film, the same lattice parameter equates to a larger strain than for a thicker one, due to the previously discussed larger influence of the surface energy.

3.2.2. Ordered stoichiometric 110 slabs

For the 110 surface, we investigate three different thicknesses, ~0.4 nm or only 3 atomic layers, ~0.8 nm with 6 atomic layers, and ~1.6 nm, or 9 atomic layers. We turn the spin-axis from the out-of-plane 110 direction to an in-plane $1\bar{1}0$ direction. (In the unstrained bulk the $1\bar{1}0$ and 110 directions are equivalent). As can be seen in Fig. 4, there are a couple of differences to the 001 slabs discussed previously: The thinner slabs do not show a transition to an in-plane easy axis, while the thickest slab exhibits an in-plane easy axis with comparatively small MCA of $< 0.5\,MJ/m^3$ at strains larger than ~2%. The maxima are much broader, and for the thickest slab its existence is actually debatable, since, in contrast to all other cases, it disappears for some reasonable smoothing factors used to construct the spline curves. For the thinner two slabs, the 0.4 nm thin one in particular, the maximum in the MCA is found at promisingly low strains of around 2.5%. This is a promising result for GMR angle sensors due to the small required strain for vanishing magnetostriction and the preservation of an out-of-plane easy axis. However, one has to note that the MCA of $0.54\,MJ/m^3$ is still extremely high for practical applications. This is an effect of the single crystal model of the thin film employed here. In order to realize soft magnetic properties magnetic grains smaller than the exchange length would be required [29].

3.3. Thin quasi-random $Fe_{10}Co_{90}$ slabs

In real world applications, like GMR sensors, FeCo alloys are typically not stoichiometric (50% Fe and 50% Co), or ordered. To investigate if the promising results achieved in the last section for ordered $Fe_{50}Co_{50}$ carry over to a more realistic system, we constructed two disordered $Fe_{10}Co_{90}$ slabs with 30 Atoms (3 Fe, 27 Co) each. While disordered films usually show larger magnetostriction than ordered ones, Co concentrations above ~80% significantly lowers magnetostriction [30,31]. To assure to simulate the disorder as well as possible in a comparatively small cell, we make use of the concept of special quasirandom structures (SQS) [32] as implemented in the ICET python package [33]. The main point of SQSs is to mimic the first few radial correlation functions of perfectly random structures much better than randomly populate supercells can if the cell dimensions are limited. In ICET, these structures are generated via simulated annealing using a Monte Carlo approach.

The SQSs for both the 001 and the 110 slabs where generated from a fully ordered stoichiometric bcc FeCo slab with 6 layers each. The cluster vectors where set up to contain pairs with interaction distance of maximal 10 Å, triplets with maximal 7.5 Å, 5.5 Å for quadruples, and 4.5 Å for quintuples. Although the initial slabs contained 6 atoms for the 001 slab and 12 for the 110 slab, the resulting SQSs both contained 30 atoms each, due to the fixed target composition of 10% Fe and 90% Co.

Since the slabs are now mainly Co, which shows a hcp crystal

[1] This analysis disregards possible changes in the magneto-elastic coupling, and the change of the elastic constants with strain.

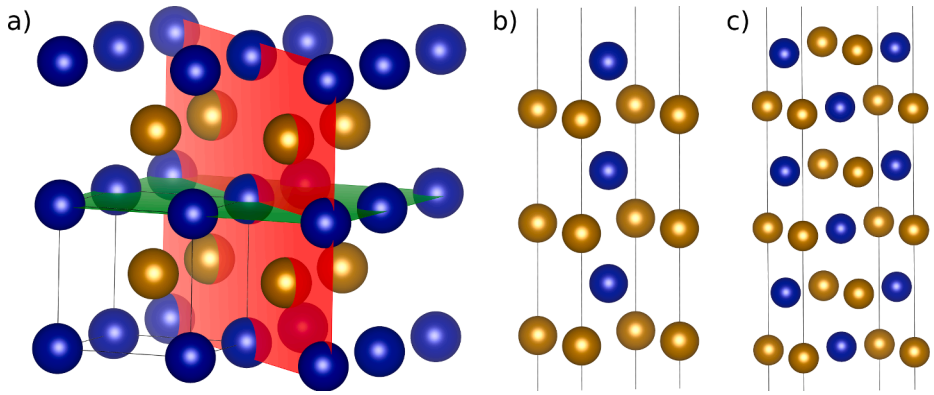

Fig. 2. Ordered B2 bulk structure of FeCo with the 001 and the 110 lattice plane highlighted in green and red, respectively (a). A 6 layer 001 slab (b) and a 6 layer 110 slab (c) are shown each without the vacuum region. Thin black lines indicate the unit cells.

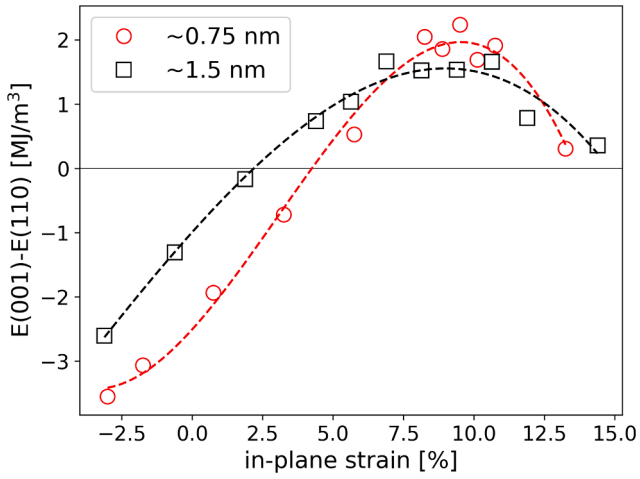

Fig. 3. MCA energy as a function of lateral strain in a and b direction of fully ordered bcc FeCo 001 slabs. The lines are smoothing splines to fit the DFT data which are shown as empty symbols. Red circles for a ~0.75 nm thick slab and black squares for a ~1.5 nm thick one..

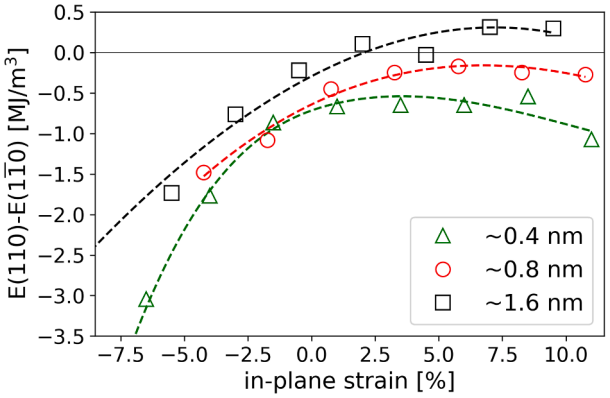

Fig. 4. MCA energy as a function of lateral strain in a and b direction of fully ordered bcc FeCo 110 slabs. The lines are smoothing splines to fit the DFT data which are shown as empty symbols. Green triangles for a ~0.4 nm thick slab, red circles for a ~0.75 nm, and black squares for a ~1.5 nm thick one.

structure with lattice parameters $a_{\mathrm{hcp}}(\mathrm{Co}) = 2.50$ Å and $c_{\mathrm{hcp}}(\mathrm{Co}) = 4.03$ Å in the ground state, it is not too surprising that the lattice parameters and maybe even the crystal structure will differ from the bcc FeCo slab we started from. For the 001 SQS slab the in-plane lattice parameter shrinks to $a_{001}(\mathrm{Fe_{10}Co_{90}}) = 2.50$ Å and the average out-of-plane lattice parameter is enlarged to $a_{001}(\mathrm{Fe_{10}Co_{90}}) = 3.42$ Å. Thus the formerly bcc structure is clearly distorted significantly with a c/a ratio of 1.369. This is quite close to the c/a ratio in a true fcc lattice of $\sqrt{2} \simeq 1.414$, and of course hcp and fcc are very closely related, being both close packed and differing only in the stacking along the 111 direction. We are not able to stabilize the bcc phase for the 001 slab because relaxations in the direction normal to the surface plane are not hindered at each lateral strain. Thus there is no separate minimum for a bcc structure observable, even if one starts from the appropriate lattice parameters. For the case of a real sensor stack, under and overlayers would probably be enough of a constraint to stabilize the bcc lattice for a $\mathrm{Fe_{10}Co_{90}}$ 001 slab, however.

In the case of the 110 surface, the change in the lattice is not as pronounced as in the 001 case. The in-plane lattice parameters are $a_{110}(\mathrm{Fe_{10}Co_{90}}) = 2.72$ Å and $b_{110}(\mathrm{Fe_{10}Co_{90}}) = 3.83$ Å, about 5% lower than for the $\mathrm{Fe_{50}Co_{50}}$, which is consistent with the significantly larger proportion of Co in the material, but the ratio $b/a = 1.41 \simeq \sqrt{2}$ is still as one would expect from a bcc 110 surface. The out-of-plane lattice parameter, however, is enlarged by ~2% to $c_{110}(\mathrm{Fe_{10}Co_{90}}) = 4.11$ Å. Since there is no easy transformation to an fcc lattice by just relaxing the atoms normal to the surface for a given strain, as was the case for the 001 slab, the stability of the bcc structure is not surprising even for a free floating thin 110 slab of $\mathrm{Fe_{10}Co_{90}}$.

3.3.1. *SQS $Fe_{10}Co_{90}$ 001 slab*

For the 001 slab model of the disordered alloy, we can see the Bains-path from the minimum structure (which is close to fcc) to a bcc crystal

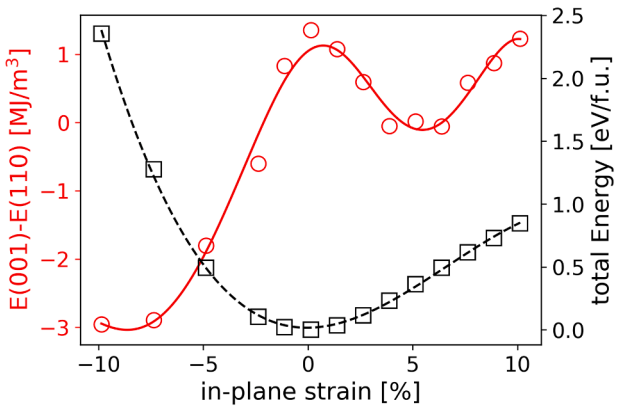

Fig. 5. MCA energy (red circles and left y-axis) and total energy (black squares and right y-axis) as a function of lateral strain in a and b direction of a SQS $\mathrm{Fe_{10}Co_{90}}$ 001 slab. The lines are smoothing splines to fit the DFT data.

reflected in the asymmetric energy vs strain curve, as can be seen in Fig. 5. We also see a complex dependency of the MCA on lateral strain. The data suggests at least one maximum and two minima in the MCA vs strain curve, with a second maximum at about ~10% strain possible. Most interesting is the maximum that we find around 0.7% strain. The easy axis is in-plane here, and the MCA is ~1.1 MJ/m^3. For an application where a relatively high MCA is desired alongside minimal or vanishing magnetostriction, such a thin film could be promising.

3.3.2. SQS $Fe_{10}Co_{90}$ 110 slab

The situation is quite different for the SQS $Fe_{10}Co_{90}$ 110 slab as shown in Fig. 6. The structure remains stable here and the energy vs strain curve is a lot more symmetrical although we still fit it with a spline to get the accurate minimum position. There is no extremum or relatively flat part in the MCA vs strain curve, but overall the curve is comparatively flat with an average slope of 0.082 MJ/m^3 per percentage point. This is more than 3 times less than for the ordered bulk structure, and nearly equivalent to the average slope of the 0.8 nm $Fe_{50}Co_{50}$ 110 slab (see the red curve in Fig. 4). Thus we can predict small, but not vanishing, magnetostriction for the disordered 110 slab. At moderate strains we predict an out-of-plane easy axis for the magnetization, switching to in-plane at around 8% expansive strain. For thicker slabs than the ~1 nm one studied here, it seems likely that the transition of the easy axis will happen at lower strains, judging from the data of the ordered stoichiometric 110 slabs.

Cabral et al. studied the effect of lateral strain on the in-plane magnetic anisotropy of thin, disordered $Fe_{20}Co_{80}$ 110 slabs both experimentally and using DFT very recently [27]. Their computational results are based on SQSs as well and a slab with 5 layers is studied, which is ~0.9 nm thick, while the experimental sample is about 20 nm thick. In the experiment the strain is applied by changing the thickness of an Au 111 underlayer.

Cabral et al. found a clear maximum in their in-plane anisotropy vs strain curve at low positive strain theoretically. The experimental accessible strain is not able to resolve that extremum, but in the accessible range the computed and measured data fit very well. Our results for $Fe_{10}Co_{90}$ suggest that at the slight positive strain where the maximum in the in-plane anisotropy is found, the easy axis is actually out-of-plane. However, we are not sure if the strain is defined in the exact same way, since Cabral et al. use an Au underlayer in the experiment and thus work with a different 0-strain lattice parameter than we do.

Combining our work with theirs, we see that the MCA of Co rich disordered FeCo alloys shows very complex strain dependence.

4. Conclusions

Our research shows that thin slabs of FeCo exhibit a complex and rich spectrum of the MCA when subjected to lateral strain. The simple linear scaling observed for the ordered bulk changes to a more complex dependence for all investigated slabs of the ordered stoichiometric alloys with maxima in the MCA vs strain curve that indicate regions of vanishing magnetostriction. Especially very thin 110 slabs have promising characteristics for GMR sensors, with broad maxima at manageable strains. The MCA at these extrema, although smaller than for other slabs, are still exceedingly large. This is however an effect of the infinite single crystal we are forced to model within DFT and in practice a small grain structure would lead to magnetically softer materials and smaller anisotropy energies. Our model slabs for disordered $Fe_{10}Co_{90}$ thin films showed us somewhat different results. For the 001 slab it was not possible to stabilize the bcc structure of the film, as it spontaneously transfers to an fcc-like film via relaxations. This film shows very complex variations to lateral strain with multiple extrema at low and high strains, some with larger and some with lower MCA. The disordered 110 $Fe_{10}Co_{90}$ slab on the other hand is stable in the bcc structure, and shows slowly varying MCA with strain without an extremum in the observed strain range. We therefore conclude that with careful selection of the film orientation, thickness, and pre-straining with a suitable substrate, the MCA of FeCo alloys can be tuned to fit a wide variety of possible applications.

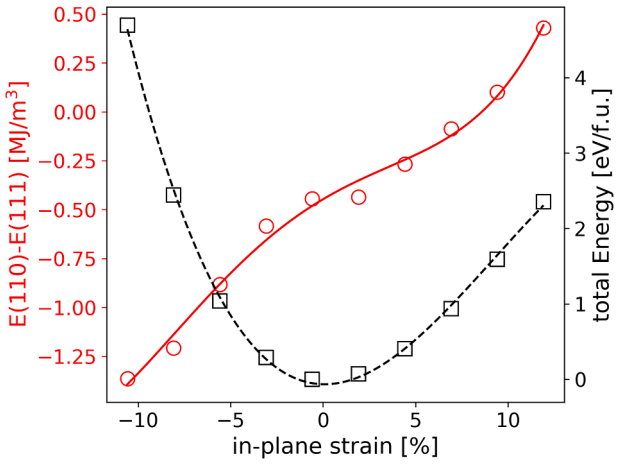

Fig. 6. MCA energy (red circles and left y-axis) and total energy (black squares and right y-axis) as a function of lateral strain in *a* and *b* direction of a SQS $Fe_{10}Co_{90}$ 110 slab. The lines are smoothing splines to fit the DFT data.

CRediT authorship contribution statement

Michael Wolloch: Conceptualization, Methodology, Formal analysis, Investigation, Data curation, Writing - original draft, Writing - review & editing, Visualization. **Dieter Suess:** Conceptualization, Resources, Writing - review & editing, Supervision, Project administration, Funding acquisition.

Declaration of Competing Interest

The authors declare that they have no known competing financial interests or personal relationships that could have appeared to influence the work reported in this paper.

Acknowledgments

We acknowledge the support from the Austrian Federal Ministry of Economy, Family and Youth, and the National Foundation for Research, Technology and Development. Michael Wolloch acknowledges the support of the Austrian Science Fund (FWF): P 32711. We also thank the Vienna Scientific Cluster (VSC) for ample computer time.

References

[1] J. Volkerts, Magnetic Thin Films: Properties, Performance, and Applications, Condensed Matter Research and Technology Series, Nova Science Publishers, Incorporated, ISBN 9781620819210, 2011. URL: https://books.google.at/books?id=GqlsAQAACAAJ.

[2] G. Scheunert, O. Heinonen, R. Hardeman, A. Lapicki, M. Gubbins, R.M. Bowman, A review of high magnetic moment thin films for microscale and nanotechnology applications, Appl. Phys. Rev. 3 (1) (2016), 011301, https://doi.org/10.1063/1.4941311.

[3] G.I. Finch, A.G. Quarrell, Crystal structure and orientation in thin films, Nature 131 (3320) (1933), https://doi.org/10.1038/131877a0, pp. 877–877, ISSN 1476–4687.

[4] W. Jesser, A theory of pseudomorphism in thin films, Mater. Sci. Eng. 4 (5) (1969) 279–286, https://doi.org/10.1016/0025-5416(69)90004-4. ISSN 0025–5416, URL: http://www.sciencedirect.com/science/article/pii/0025541669900044.

[5] W. Granig, M. Weinberger, C. Reidl, M. Bresch, M. Strasser, G. Pircher, G.M. R. Integrated, angle sensor for electrical commutated motors including features for safety critical applications, Procedia Engineering 5, 1384–1387, ISSN 1877–7058 (2010), https://doi.org/10.1016/j.proeng.2010.09.373. URL: http://www.sciencedirect.com/science/article/pii/S1877705810009203, eurosensor XXIV Conference.

[6] R.C. Hall, Magnetic anisotropy and magnetostriction of ordered and disordered cobalt-iron alloys, J. Appl. Phys. 31 (5) (1960) S157–S158, https://doi.org/10.1063/1.1984643.
[7] M. Staruch, D.B. Gopman, Y.L. Iunin, R.D. Shull, S.F. Cheng, K. Bussmann, P. Finkel, Reversible strain control of magnetic anisotropy in magnetoelectric heterostructures at room temperature, Scientific Rep. 6 (1) (2016) 37429, https://doi.org/10.1038/srep37429.
[8] G. Engdahl, Handbook of Giant Magnetostrictive Materials, Academic Press, Oxford, San Diege, CA, 2000.
[9] G. Kresse, J. Hafner, Ab initio molecular dynamics for liquid metals, Phys. Rev. B 47 (1993) 558–561, https://doi.org/10.1103/PhysRevB.47.558.
[10] G. Kresse, J. Furthmüller, Efficiency of ab-initio total energy calculations for metals and semiconductors using a plane-wave basis set, Comput. Mater. Sci. 6(1) (1996) 15–50.https://doi.org/10.1016/0927-0256(96)00008-0, ISSN 0927–0256. URL: http://www.sciencedirect.com/science/article/pii/0927025696000080.
[11] G. Kresse, J. Furthmüller, Efficient iterative schemes for ab initio total-energy calculations using a plane-wave basis set, Phys. Rev. B 54 (1996) 11169–11186, https://doi.org/10.1103/PhysRevB.54.11169.
[12] P.E. Blöchl, Projector augmented-wave method, Phys. Rev. B 50 (1994) 17953–17979, https://doi.org/10.1103/PhysRevB.50.17953.
[13] G. Kresse, D. Joubert, From ultrasoft pseudopotentials to the projector augmented-wave method, Phys. Rev. B 59 (1999) 1758–1775, https://doi.org/10.1103/PhysRevB.59.1758.
[14] F. Birch, Finite elastic strain of cubic crystals, Phys. Rev. 71 (1947) 809–824, https://doi.org/10.1103/PhysRev.71.809.
[15] P. Wisesa, K.A. McGill, T. Mueller, Efficient generation of generalized Monkhorst-Pack grids through the use of informatics, Phys. Rev. B 93 (2016), 155109, https://doi.org/10.1103/PhysRevB.93.155109.
[16] J.P. Perdew, K. Burke, M. Ernzerhof, Generalized gradient approximation made simple, Phys. Rev. Lett. 77 (1996) 3865–3868, https://doi.org/10.1103/PhysRevLett.77.3865.
[17] Y. Fu, D.J. Singh, Density functional methods for the magnetism of transition metals: SCAN in relation to other functionals, Phys. Rev. B 100 (2019), 045126, https://doi.org/10.1103/PhysRevB.100.045126.
[18] M. Methfessel, A.T. Paxton, High-precision sampling for Brillouin-zone integration in metals, Phys. Rev. B 40 (1989) 3616–3621, https://doi.org/10.1103/PhysRevB.40.3616.
[19] K. Umadevi, J. Arout Chelvane, A. Talapatra, J. Mohanty, V. Jayalakshmi, Interplay of magnetic anisotropies on the magnetostrictive behavior of Fe–Co thin films, J. Mater. Sci.: Mater. Electron. 29 (20) (2018) 17714–17721, https://doi.org/10.1007/s10854-018-9877-3. ISSN 1573–482X.
[20] T. Sourmail, Near equiatomic FeCo alloys: constitution, mechanical and magnetic properties, Prog. Mater. Sci. 50 (7) (2005) 816–880, https://doi.org/10.1016/j.pmatsci.2005.04.001. ISSN 0079–6425. URL: http://www.sciencedirect.com/science/article/pii/S0079642505000204.
[21] M. Getzlaff, Fundamentals of Magnetism, Springer, 2008, ISBN 9783540311508, URL: https://books.google.at/books?id=RNgBmQEACAAJ.
[22] T. Burkert, L. Nordström, O. Eriksson, O. Heinonen, Giant magnetic anisotropy in tetragonal FeCo alloys, Phys. Rev. Lett. 93 (2004), 027203, https://doi.org/10.1103/PhysRevLett.93.027203.
[23] E.K. Delczeg-Czirjak, A. Edström, M. Werwiski, J. Rusz, N.V. Skorodumova, L. Vitos, O. Eriksson, Stabilization of the tetragonal distortion of Fe_xCo_{1-x} alloys by C impurities: a potential new permanent magnet, Phys. Rev. B 89 (2014), 144403, https://doi.org/10.1103/PhysRevB.89.144403.
[24] I. Khan, J. Hong, Magnetic anisotropy of C and N doped bulk FeCo alloy: a first principles study, J. Magn. Magn. Mater. 388 (2015) 101–105, https://doi.org/10.1016/j.jmmm.2015.04.021. URL: http://www.sciencedirect.com/science/article/pii/S0304885315300317.
[25] L. Reichel, L. Schultz, D. Pohl, S. Oswald, S. Fhler, M. Werwiński, A. Edstrm, E. K. Delczeg-Czirjak, J. Rusz, From soft to hard magnetic Fe–Co–B by spontaneous strain: a combined first principles and thin film study, J. Phys.: Condens. Matter 27 (47) (2015), 476002, https://doi.org/10.1088/0953-8984/27/47/476002.
[26] M. Wolloch, G. Losi, M. Ferrario, M.C. Righi, High-throughput screening of the static friction and ideal cleavage strength of solid interfaces, Scientific Rep. 9 (1) (2019) 17062, https://doi.org/10.1038/s41598-019-49907-2.
[27] L. Cabral, F.H. Aragn, L. Villegas-Lelovsky, M.P. Lima, W.A.A. Macedo, J.L.F. Da Silva, Tuning the magnetic properties of FeCo thin films through the magnetoelastic effect induced by the Au underlayer thickness, ACS Appl. Mater. Interfaces 11 (1) (2019) 1529–1537, https://doi.org/10.1021/acsami.8b14736.
[28] L. Reichel, A. Edstrm, D. Pohl, J. Rusz, O. Eriksson, L. Schultz, S. Fhler, On the origin of perpendicular magnetic anisotropy in strained Fe–Co(–X) films, J. Phys. D: Appl. Phys. 50 (4) (2017), 045003, https://doi.org/10.1088/1361-6463/aa51af.
[29] G. Herzer, Nanocrystalline soft magnetic materials, J. Magn. Magn. Mater. 112 (1) (1992) 258–262, https://doi.org/10.1016/0304-8853(92)91168-S. ISSN 0304–8853, URL: http://www.sciencedirect.com/science/article/pii/030488539291168S.
[30] D. Hunter, W. Osborn, K. Wang, N. Kazantseva, J. Hattrick-Simpers, R. Suchoski, R. Takahashi, M.L. Young, A. Mehta, L.A. Bendersky, S.E. Lofland, M. Wuttig, I. Takeuchi, Giant magnetostriction in annealed Co1–Fex thin-films, Nat. Commun. 2 (1) (2011) 518, https://doi.org/10.1038/ncomms1529.
[31] S. ichi Yamaura, T. Nakajima, T. Satoh, T. Ebata, Y. Furuya, Magnetostriction of heavily deformed Fe–Co binary alloys prepared by forging and cold rolling, Mater. Sci. Eng.: B 193 (2015) 121–129, https://doi.org/10.1016/j.mseb.2014.12.009. ISSN 0921-5107, URL: http://www.sciencedirect.com/science/article/pii/S092151071400275X.
[32] A. Zunger, S.-H. Wei, L.G. Ferreira, J.E. Bernard, Special quasirandom structures, Phys. Rev. Lett. 65 (1990) 353–356, https://doi.org/10.1103/PhysRevLett.65.353.
[33] M. Ångqvist, W.A. Muñoz, J.M. Rahm, E. Fransson, C. Durniak, P. Rozyczko, T. H. Rod, P. Erhart, ICET – a python library for constructing and sampling alloy cluster expansions, Adv. Theory Simul. 2 (7) (2019) 1900015, https://doi.org/10.1002/adts.201900015.